

Does the Earth Have an Adaptive Infrared Iris?



Richard S. Lindzen,* Ming-Dah Chou,+ and Arthur Y. Hou[†]

ABSTRACT

Observations and analyses of water vapor and clouds in the Tropics over the past decade show that the boundary between regions of high and low free-tropospheric relative humidity is sharp, and that upper-level cirrus and high free-tropospheric relative humidity tend to coincide. Most current studies of atmospheric climate feedbacks have focused on such quantities as clear sky humidity, average humidity, or differences between regions of high and low humidity, but the data suggest that another possible feedback might consist of changes in the relative areas of high and low humidity and cloudiness. Motivated by the observed relation between cloudiness (above the trade wind boundary layer) and high humidity, cloud data for the eastern part of the western Pacific from the Japanese *Geostationary Meteorological Satellite-5* (which provides high spatial and temporal resolution) have been analyzed, and it has been found that the area of cirrus cloud coverage normalized by a measure of the area of cumulus coverage decreases about 22% per degree Celsius increase in the surface temperature of the cloudy region. A number of possible interpretations of this result are examined and a plausible one is found to be that cirrus detrainment from cumulus convection diminishes with increasing temperature. The implications of such an effect for climate are examined using a simple two-dimensional radiative-convective model. The calculations show that such a change in the Tropics could lead to a negative feedback in the global climate, with a feedback factor of about -1.1 , which if correct, would more than cancel all the positive feedbacks in the more sensitive current climate models. Even if regions of high humidity were not coupled to cloudiness, the feedback factor due to the clouds alone would still amount to about -0.45 , which would cancel model water vapor feedback in almost all models. This new mechanism would, in effect, constitute an adaptive infrared iris that opens and closes in order to control the Outgoing Longwave Radiation in response to changes in surface temperature in a manner similar to the way in which an eye's iris opens and closes in response to changing light levels. Not surprisingly, for upper-level clouds, their infrared effect dominates their shortwave effect. Preliminary attempts to replicate observations with GCMs suggest that models lack such a negative cloud/moist areal feedback.

1. Introduction

We begin with a general overview of atmospheric feedbacks in order to establish the context for emphasizing the feedback arising from changes in the area

of cloudy moist air, which we will refer to as the iris effect.

Our current intuitions concerning both the greenhouse effect and the role of atmospheric feedbacks owe much to the one-dimensional models of the sort used by Manabe and Wetherald (1967). Here, the atmosphere is characterized by a single vertical distribution of water vapor, and a specified mean cloud cover consisting in clouds at one or more levels. However, in recent years, satellites have provided detailed pictures of the horizontal distribution of water vapor at various levels. Figure 1 illustrates such a distribution obtained by Spencer and Braswell for 5 May 1995 for the layer 500–300 mb from 183-GHz microwave radiation observed from the Special Sensor Microwave Water Vapor Sounder (SSM/T-2) military satellite. [Spencer and Braswell (1997) show similar results for

*Department of Earth, Atmospheric and Planetary Sciences, Massachusetts Institute of Technology, Cambridge, Massachusetts.

[†]Laboratory for Atmospheres, NASA Goddard Space Flight Center, Greenbelt, Maryland.

Corresponding author address: Dr. Richard S. Lindzen, Department of Earth, Atmospheric, and Planetary Sciences, Massachusetts Institute of Technology, Room 54-1720, Cambridge, MA 02139.

E-mail: rlindzen@mit.edu

In final form 29 September 2000.

©2001 American Meteorological Society

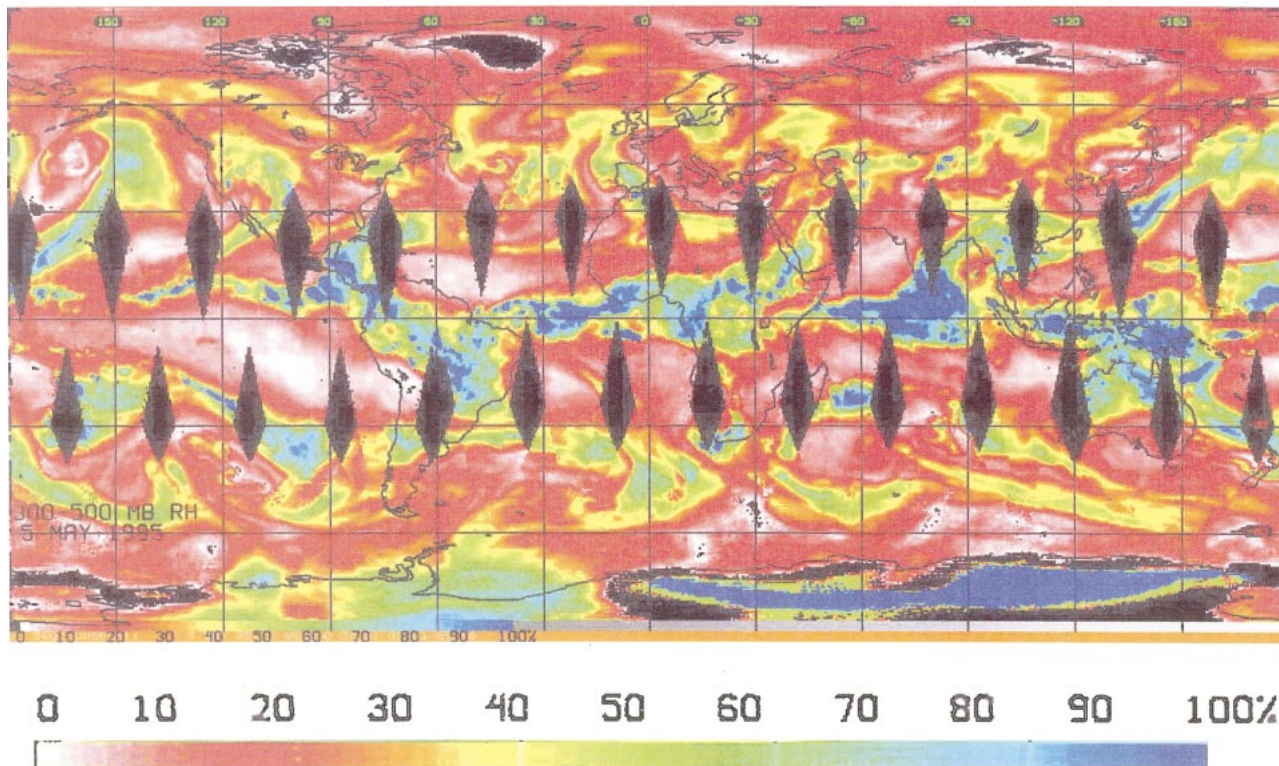


FIG. 1. Retrieval of relative humidity for the 500–300-mb layer on 5 May 1995 from SSM/T-2 183-GHz soundings. Courtesy of R. Spencer. See Spencer and Braswell (1997) for details of the observing and retrieval procedure.

a monthly mean; however, we wished to show a daily map as opposed to a monthly mean since radiation responds to the instantaneous distribution.] Although microwave retrievals are less sensitive to the presence of clouds, similar results were obtained from Television Infrared Observation Satellite (TIROS) Operational Vertical Sounder infrared soundings (Stephens et al. 1996). Results for all levels above 700 mb are similar. Below 700 mb we have the turbulent trade wind boundary layer in the Tropics where humidity tends to be relatively high everywhere. What we see is that the Tropics above the boundary layer is made up of regions that are very dry and regions that are very moist. The transition between the two is sharp; this sharpness is not so apparent in monthly means. In view of the sharp transition between moist and dry regions, a focus on average humidity in assessing feedbacks may be misleading.

The dry regions are generally regions of large-scale subsidence. The moist regions are more complicated. While they tend to be regions of large-scale ascent, the ascent is concentrated in cumulus towers that have small areal coverage (Riehl and Malkus 1958; Held and Soden 2000). The bulk of the moist regions consists in descending air that is moistened by the evapo-

ration of precipitation from high cirrus and, at levels below about 500 mb, by dissipating cumuli (Gamache and Houze 1983; Betts 1990; Sun and Lindzen 1993). In general, in the Tropics, high stratiform clouds are the source of high humidity, and the production of high cirrus depends on the microphysics of rain formation within the cumulus towers (Emanuel and Pierrehumbert 1996; Sun and Lindzen 1993). Condensed water vapor that does not form rain freezes and is available to form cirrus outflow. The situation is schematically illustrated in Fig. 2. Although Fig. 2 shows only cirrus outflow near the top, in reality the outflow occurs over a broad range of heights.

Consistent with the role of high cirrus clouds in moisturizing the tropical troposphere, Udelhofen and Hartmann (1995) find a close correspondence between upper-level cloudiness and high relative humidity. For monthly means, they find that high relative humidity is confined to within 500 km of the cloudy regions. However, for daily retrievals the correspondence is tighter, though precise determination is limited by data resolution. Radiation, of course, responds to the instantaneous values of radiatively active substances rather than to their means. High clouds can be measured with high spatial and temporal resolution from geostation-

ary satellites. The measurement of relative humidity, on the other hand, is difficult in the presence of clouds and requires somewhat ambiguous “cloud clearing” algorithms. The above results, however, suggest that upper-level cloudiness might serve as a surrogate for high relative humidity, thus obviating the need to explicitly measure the area of high humidity. We are currently examining this issue using data from the Clouds and Earth Radiant Energy System (CERES) instrument on the Tropical Rainfall Measuring Mission (TRMM) satellite, but the full results will be published separately. Note that in this view, the traditional cloud and water vapor feedbacks are inextricably tied to each other though the moist region is not at all totally cloud covered, and it should be noted that the radiative properties of the cloudy moist regions will, of course, differ from those of the clear moist regions.

A number of recent studies (Sherwood 1996; Soden 1998; Salathé and Hartmann 1997; Pierrehumbert and Roca 1998) have shown that in the dry regions of Fig. 1 the water vapor budget is in largely advective balance with no evidence of any other sources at all. This limits the possibilities for altering the humidity of dry regions. In addition, the moist tropical regions in Fig. 1 are very moist though not necessarily near saturation.

In this paper, we will not examine how moisture might change within the moist and dry regions. Rather, we will focus on the remaining possibility of a feedback residing in changing the relative areas of moist and dry air in response to changes in surface temperature. In calculations of feedbacks that would be associated with this effect, we will hold humidity fixed within the dry and moist regions (or more precisely, we fix emission levels). Since feedback factors are additive (see discussion in section 4), we can examine the additional effect of feedbacks found in GCM results by simply adding their feedback factors to that of the area effect. Given the sharp transition between moist and dry regions shown in Fig. 1, we may plausibly expect that shrinking (growing) moist areas are accompanied by growing (shrinking) dry areas. In section 2, we discuss the area feedback in more detail, and in section 3, we describe how we can use high-resolution cloud observations to evaluate this feedback, and present some preliminary results for the period January 1998–August 1999. The observationally based coincidence of cloudy and moist regions is utilized in the subsequent theoretical analysis, but the consequences of decoupling the two is examined as well in order to isolate the specific effect of

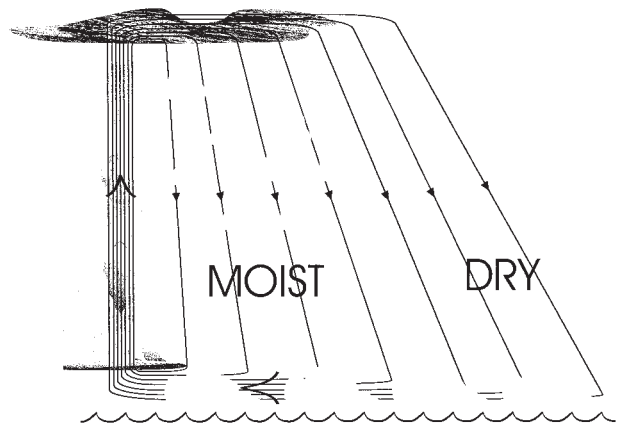


FIG. 2. Schematic illustrating the moisturization of underlying air by precipitation from cirrus outflow of cumulonimbus clouds.

varying cloud area. A very strong inverse relation is found between cloud area and the mean SST of cloudy regions (which we refer to as the cloud-weighted SST). Ambiguities in the interpretation of the data are discussed as well. However, we argue that a plausible interpretation is that the results reflect a temperature dependence for the cirrus detrainment from cumulus towers. This dependence appears to act as an *iris* (by analogy with the eye’s iris) that opens and closes dry regions so as to inhibit changes in surface temperature (in contrast to the eye’s iris, which does the same in order to counter changes in light intensity). Section 4 uses a simple two-dimensional radiative–convective model to estimate climate feedbacks following from this interpretation; this section also includes a reexamination of the relation of the area of moist air to the area of cloudy air. Section 5 compares the observed behavior with the behavior of GCMs. Section 6 discusses possible implications for climate as well as the limitations of the present analysis.

2. Discussion of the area feedback

In considering the feedback in the Tropics that might result from changes in the relative areas of the dry and moist regions, one should note that dynamics effectively homogenizes temperature in the horizontal, so that the dry regions act to cool the whole Tropics. Such a situation was graphically described by Pierrehumbert (1995) among others. Eddies act to couple the Tropics to the rest of the globe.

An area feedback hinges on the factors that determine cirrus detrainment from cumulus towers. In general, detrainment of ice depends on the water substance

carried by cumulus updrafts that is *not* rained out within the tower. This is determined by a competition between processes determining the rate of rain formation, and processes such as convective available potential energy (CAPE), which determine the time available for rain formation. Feedbacks will depend on the specific impact of surface temperature. Sun and Lindzen (1993), using the simple Bowen model for coalescence (*viz.*, Rogers and Yau 1989, p. 131), and assuming that cloud water content increases as surface humidity increases (which for a given size spectrum of cloud water implies more cloud water droplets to feed the growth of raindrops through coalescence as well as providing more water vapor for condensation) found that the growth rate of raindrops increased 15% for a 2°C increase in surface temperature (assuming fixed relative humidity in the boundary layer). The Bowen mechanism may well underestimate this effect. Such processes as stochastic coalescence accelerate raindrop formation nonlinearly. Moreover, the drag exerted on cloud updrafts by falling rain would allow more time for rain formation. Thus, the possibility exists that precipitation efficiency within cumulus towers can increase significantly with increasing surface temperature thus reducing cirrus outflow. To be sure, temperature is not the only factor determining precipitation efficiency within cumulus towers—a point we will return to later.

Rather than attempt to deal with the complexities of the cloud physics, we will try to determine the existence and magnitude of the area feedback directly from the data. We will examine how the area covered by upper-level cirrus varies with the average temperature of the cloud-covered regions. Essentially, we are looking at the average surface temperature weighted according to cloud coverage. We weight the temperature according to cloud coverage because cloud microphysics depends on the temperature beneath the clouds and not the average temperature over the whole domain. The origin of such temperature changes depends upon, among other things, the time interval considered. Thus, over short periods of a week or so, SST varies relatively little (over most regions), and cloud-weighted SST changes mostly due to clouds, whose lifetimes are measured in hours, popping up in different locations characterized by different SSTs as illustrated *schematically* in Fig. 3. Over longer periods, the situation is more complex. Not only are there changes in SST, but changing patterns in surface temperature (Lindzen and Nigam 1987) and propagating internal waves (Miller and Lindzen 1992;

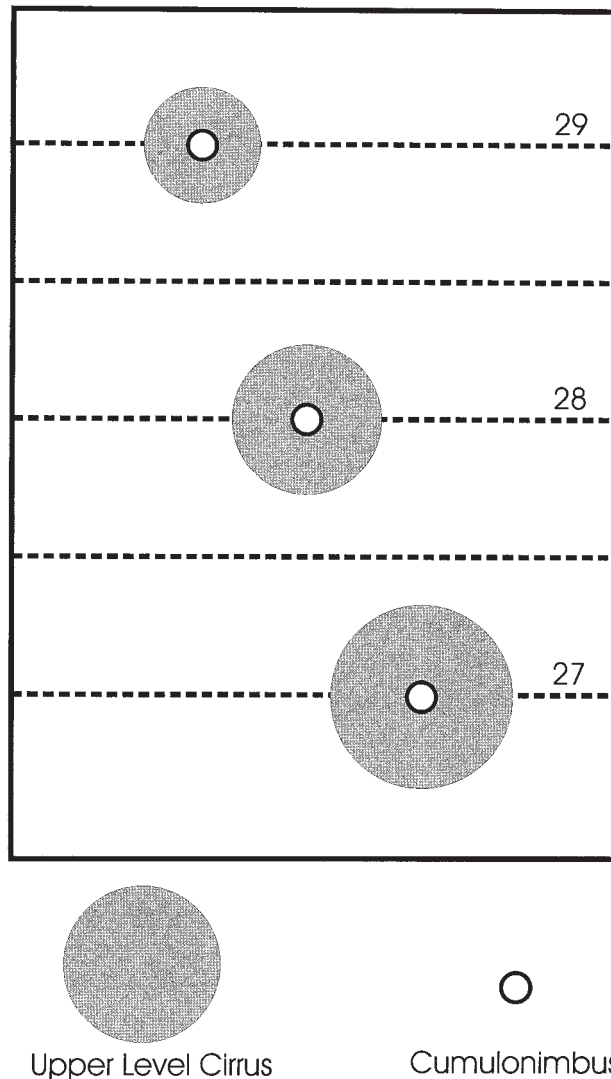


FIG. 3. Schematic illustrating change in cloud-weighted SST due to cloud systems moving from the central position to colder and warmer regions. Dotted horizontal lines correspond to isotherms. Units are nominally °C.

Straus and Lindzen 2000) lead to varying distributions of low-level convergence and shifting patterns of convection.

Theoretically, given the short timescales associated with cloud processes, it seems likely that the dependence of the area of moist air on cloud-weighted SST should not depend greatly on the specific origin of the changes in cloud-weighted SST (*i.e.*, whether the temperature changes were associated with varying positions of clouds or with actual changes in SST). However, within limited regions, the seasonal and interseasonal changes in regime can, in principle, alter the overall level of convection within the region. We will attempt to account for this by normalizing

cirrus area by cumulus area, making use of the fact that the two correspond to different cloud brightness temperatures. We expect that the area of moist air will be proportional to the area of cloudy air. However, we lack supporting data comparable in time and space resolution to our cloud data and, hence, cannot be sure that the proportionality is simple. In our theoretical analysis we will consider a variety of possibilities.

A question may be raised as to the relevance of using data over only 20 months to assess feedbacks for global change. For timescales of months to years (including ENSO), changes in SST are spatially irregular, and there need be no particular relation between changes in cloud-weighted SST and domain-averaged surface temperature, though increases in domain-averaged SST will, of course, contribute to cloud-weighted SST. Indeed, as we will note in section 3, the latter can be much larger than the former. However, for global change due to doubling CO_2 , global mean temperature should be a suitable measure for cloud-weighted SST since presumably almost all temperatures are proportional (at least in models). Even here, the physically relevant temperature change for the area of the moist region will be the cloud-weighted surface temperature. It bears emphasizing that the physics (precipitation formation, etc.) determining the area of the moist regions is fast, and hence such changes in area can be measured from short period fluctuations. However, it is the same fast physics that determines the response to long period fluctuations.

3. Explicit observational results

We wish next to examine the data to determine whether a significant feedback exists in the form of a response of the area of cloudy air to changes in the cloud-weighted SST. An advantage of measuring clouds is the existence of 11- and 12- μm channels, which can be used to detect clouds (Prabhakara et al. 1993) on geostationary satellites that obtain data with high temporal and spatial resolution over fixed regions. Unfortunately, archives of most such data are not readily available. However, we have been able to archive data from the Japanese Geostationary Meteorological Satellite (GMS) since January 1998. When clouds are viewed with high time and space resolution, they appear very patchy with the patches moving about very substantially over short periods. Given the physics illustrated in Fig. 2, we expect that these clouds will moisturize the air between close by patches. Thus we

expect some proportionality between cloud area and the area of moist air; however, it is by no means clear that the percentage change in the area of moist air will be the same as the percentage change in cloudy air—especially given the somewhat arbitrary choices of threshold temperatures. Since our aim is not so much to produce a definitive analysis as to obtain some idea of the existence and magnitude of the effect, we will examine a range of possibilities.

The situation with respect to surface temperature is somewhat more problematic. The primary available dataset is the National Centers for Environmental Prediction (NCEP) data compiled by Reynolds and Smith (1994) from ship track and satellite observations. The SST is smoothly varying and does not change much within a $1^\circ \times 1^\circ$ region. Although there are regions where SST has a significant diurnal variation (at least in skin temperature) that is not accounted for here (Fairall et al. 1996), the magnitude of the diurnal variation is smaller than the large-scale SST variation. Furthermore, the air temperature is more relevant for cloud microphysics, and this temperature has a smaller diurnal variation.

We have, so far, examined high cloud over the region 30°S – 30°N , 130°E – 170°W using cloud data from GMS-5 and NCEP SST for 20 months (1 Jan 1998–31 Aug 1999). The region is shown in Fig. 4. The region encompasses a wide variety of situations—especially in the course of 20 months. For a heavily ocean-covered region, we may plausibly expect clouds to be responding to surface temperature; over land, the situation is likely to be more complicated since surface temperatures can respond rapidly to clouds. We, therefore, restrict ourselves to the simpler oceanic regions in this paper.

Japan's GMS is located above the equator and 140°E longitude. To estimate high-level cloud coverage both day and night, only the brightness temperatures measured at the split-window channels (11 and 12 μm) are used. A GMS pixel is determined to be totally covered by high clouds if the brightness temperatures at the 11- μm channel (T_{11}) is less than a subjectively selected threshold temperature, T_{th} . For thick high clouds, the difference between the brightness temperatures at the 12- μm channel (T_{12}) and T_{11} is small, which can be used to differentiate thick clouds from thin clouds (Prabhakara et al. 1993). This threshold temperature difference, dT , depends upon the spectral ranges of the split-window channels. For the GMS channels, clouds are empirically determined to be thick if the temperature difference, dT , is less than 1.5 K.

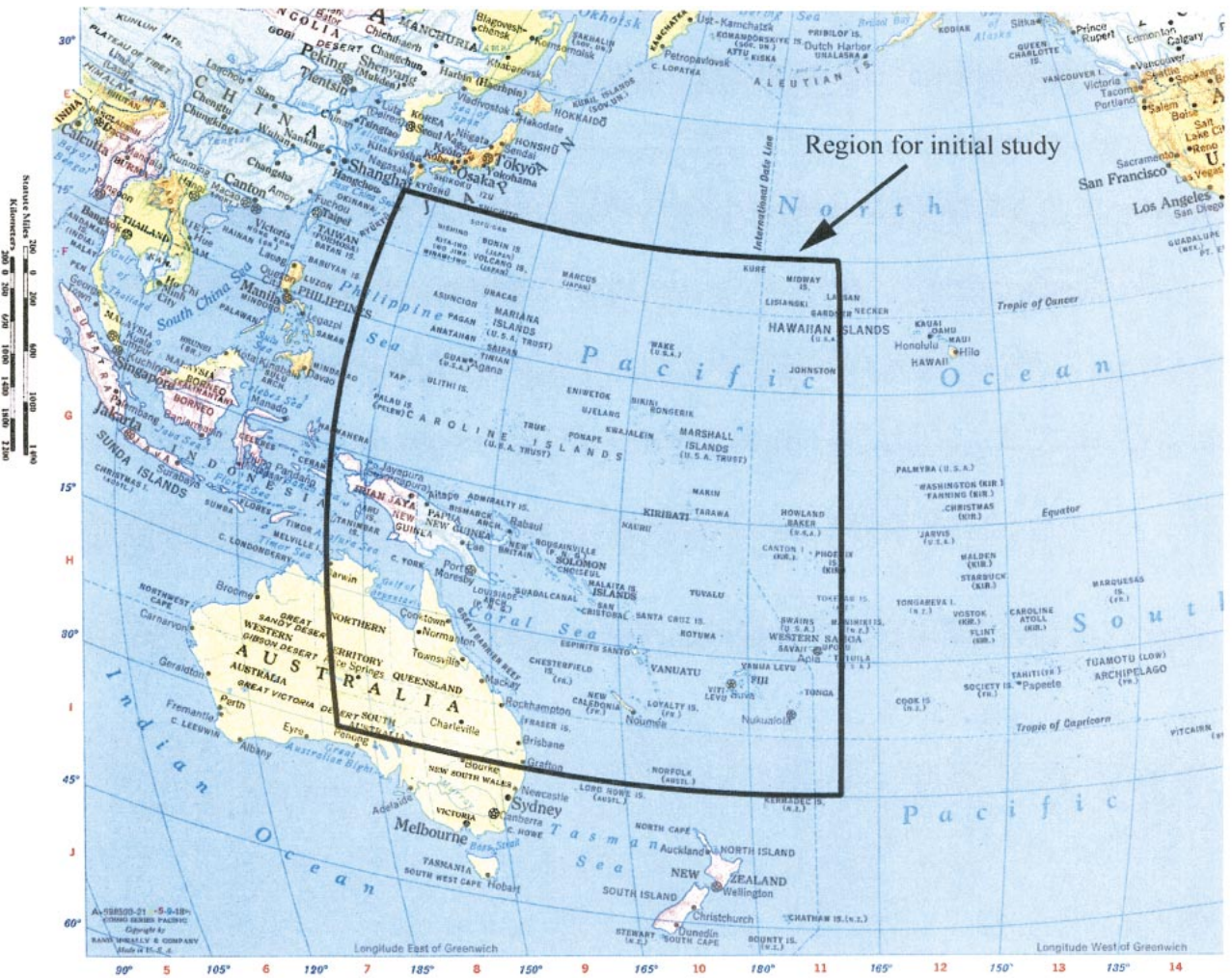


Fig. 4. Region used for present study.

Hourly high cloud area in a $1^\circ \times 1^\circ$ latitude–longitude region is estimated using the 5-km resolution pixels.

The displacement of cloud systems depends on large-scale conditions. The timescale of clouds is much smaller than that of the SST. When the cloud systems appear in a warm oceanic region, they are expected to be modified by the SST nearly immediately. SST will also respond to clouds, but at a much slower pace. Thus, the modification of clouds by local SST can be studied by correlating high cloud area to the local SST.

For a large oceanic domain, the mean high-cloud amount (area) and the mean SST beneath high clouds are computed from

$$A = \frac{\sum_n A_n \cos \theta_n}{\sum_n \cos \theta_n}$$

and

$$\bar{T} = \frac{\sum_n A_n T_n \cos \theta_n}{\sum_n A_n \cos \theta_n},$$

where A is the cloud amount (area), T is the SST, θ is the latitude, and the subscript n denotes $1^\circ \times 1^\circ$ latitude–longitude regions.

The results for the 20-month period are shown in Figs. 5a and 5b. Figure 5a corresponds to channel 11's brightness temperature being less than 260 K, corresponding to upper-level clouds, while Fig. 5b shows the subset of clouds in Fig. 5a for which the channel 12 brightness temperature is within 1.5 K of Channel 11, which, as we discussed earlier, corresponds to thicker clouds. Several points should be noted: 1) there is a substantial scatter to the points, which is to be

expected since precipitation efficiency does not depend only on temperature; our interest is in whether there is a discernible and statistically significant dependence on temperature that emerges from the scatter; 2) the coverage of thicker clouds is considerably less than the coverage of all clouds; and 3) Figs. 5a and 5b both show a reduction of cloud amount (area) by about 15% per 1-K increase in cloud-weighted SST, which suggests that both measures are proportional to overall cloudiness. A straightforward statistical analysis of the results shows that the standard deviation for the slope amounts to about 11%. In other words, using 3 times the standard deviation as our uncertainty, the decrease for an increase of 1 K in cloud-weighted SST lies between 10% and 20%.

One interpretation of Figs. 5a and 5b is that detrainment diminishes with cloud-weighted surface temperature.

However, this is hardly the only interpretation. For example, changes in high cloud area might be associated with changes in the amount of cumulus convection (as might be caused by changes in low-level convergence due to either seasonal changes in SST pattern or the penetration into the Tropics of extratropical systems) rather than in changes in detrainment from cumulus. To test for this possibility we examine the dependence of cloud coverage for channel 11 brightness temperature less than 220 K. Here we are looking primarily at the cold tops of cumulonimbus towers, and for the purposes of this initial study, that is how we will interpret this measure. However, it should be clear that this measure is approximate at best since there are also stratiform clouds associated with such low brightness temperatures, and there are cumulus towers associated with higher brightness temperatures. The results are shown in Fig. 5c. We do not show results for thicker clouds since these did not differ from what is shown in Fig. 5c; that is, all these clouds are thick. We no longer see a clear reduction with increasing cloud-weighted temperature; indeed there is a small increase. This supports the identification of what we see in Figs. 5a and 5b as being mostly due to varying detrainment from cumulus convection rather than any change in the amount of cumulus convection it-

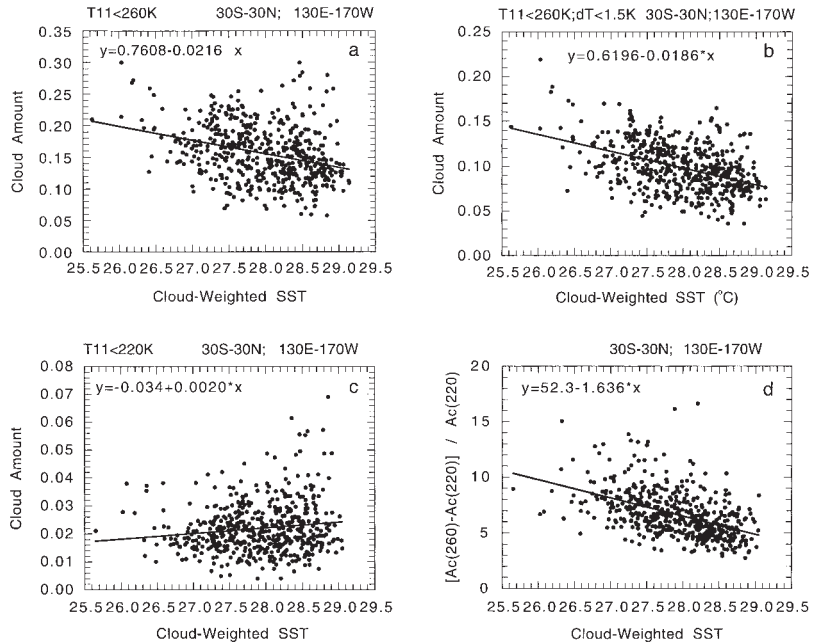


FIG. 5. Scatterplots showing how cirrus coverage varies with cloud-weighted SST for both “all” (a) upper-level clouds and (b) thick clouds. Also shown is (c) the variation of cumulus area with cloud-weighted SST and (d) the variation of cirrus coverage normalized by cumulus coverage. Data points correspond to daily averages. (See text for details.)

self. Indeed, the fact that cumulus convection appears to have been increasing somewhat, suggests that the area effect in Figs. 5a and 5b is likely to be *underestimated*, since increasing convection would generally lead to more rather than less upper-level cloudiness (since the cumuli are the primary source for upper-level clouds, which are primarily cirrus). The areal coverage for cumulus towers even within the cloudy regions is small (ca 2%)—especially when one considers that at any given moment most cumulus tops represent dying rather than active cumulus.

A more useful diagnostic of the detrainment effect would be the area of high cloud normalized by the area of cumulus. This is shown in Fig. 5d. Here, we see that the scatter is reduced, and the area of high cloud per unit area of cumulus decreases by about 22% per degree Celsius increase in cloud-weighted SST. Reflecting the reduced scatter, the standard error for the slope is about 8%. Again using 3 times the standard deviation as our uncertainty, the decrease for an increase of 1 K in cloud-weighted SST lies between 17% and 27%.

A potential problem here is that area may not be a reliable measure of cumulus activity. The mass flux in cumulus towers, M_c , is given by $M_c = \rho_c w_c A_c$, where ρ_c , w_c , and A_c are the density, mean vertical velocity, and

and the area of the cumulus convection. Changing M_c might result from changing w_c as well as A_c (as might

occur for changes in CAPE—a matter discussed later in this paper). If we refer to the area of high stratiform cloud as A_s , then $(A_s/M_c)=(A_s/A_c)(l/\rho_c w_c)$; w_c is generally reckoned as more likely to increase than to decrease with increasing SST. Therefore, the results shown in Fig. 5d are likely to lead to underestimating the detrainment effect.

The utility of the normalized area as a diagnostic becomes especially clear if we restrict ourselves to regions where we can be certain that temperature changes are associated with shifting patterns of convection. This is the case, for example, for regions restricted to one side of the equator. Seasonal changes involving the motion of the ITCZ no longer cancel out as they tend to when both sides of the equator are considered. Thus, in Fig. 6a we see the same sort of scatter diagram as in Fig. 5a, but for the region 15°S–equator. Now, the stratiform high cloud area is increasing with cloud-weighted temperature in distinct contrast to Fig. 5a. In Fig. 6b we show the counterpart of Fig. 5c for the new region. Here we see that the area of deep cumulus is also increasing with cloud-weighted temperature. The points in Figs. 6a and 6b with low cloud-weighted SST and low fractional cloud amount come from those days in the southern winter months when the ITCZ is north of the equator. The opposite is true for the points with high SST, which correspond to those days when the ITCZ is south of the equator in the southern summer months. However, in Fig. 6c (the counterpart of Fig. 5d) we see that the ratio A_s/A_c decreases with cloud-weighted temperature approximately as it does in Fig. 5d.

It should be noted that Figs. 5d and 6c suggest that a simple linear regression may not be entirely appropriate. Indeed, the variation seems more rapid at lower temperatures and larger areal coverage—consistent with the interpretation as a percentage change per degree Celsius change in cloud-weighted SST. This is confirmed by plotting the log of the ratio A_s/A_c (not shown). Now, the cluster of points all follow a linear pattern with a slope corresponding to $-24.7\% \pm 5.6\%$ per degree Celsius (for the case considered in Fig. 5d), and to $-38.7\% \pm 10.95\%$ per degree Celsius (for the case considered in Fig. 6c). In general, these results

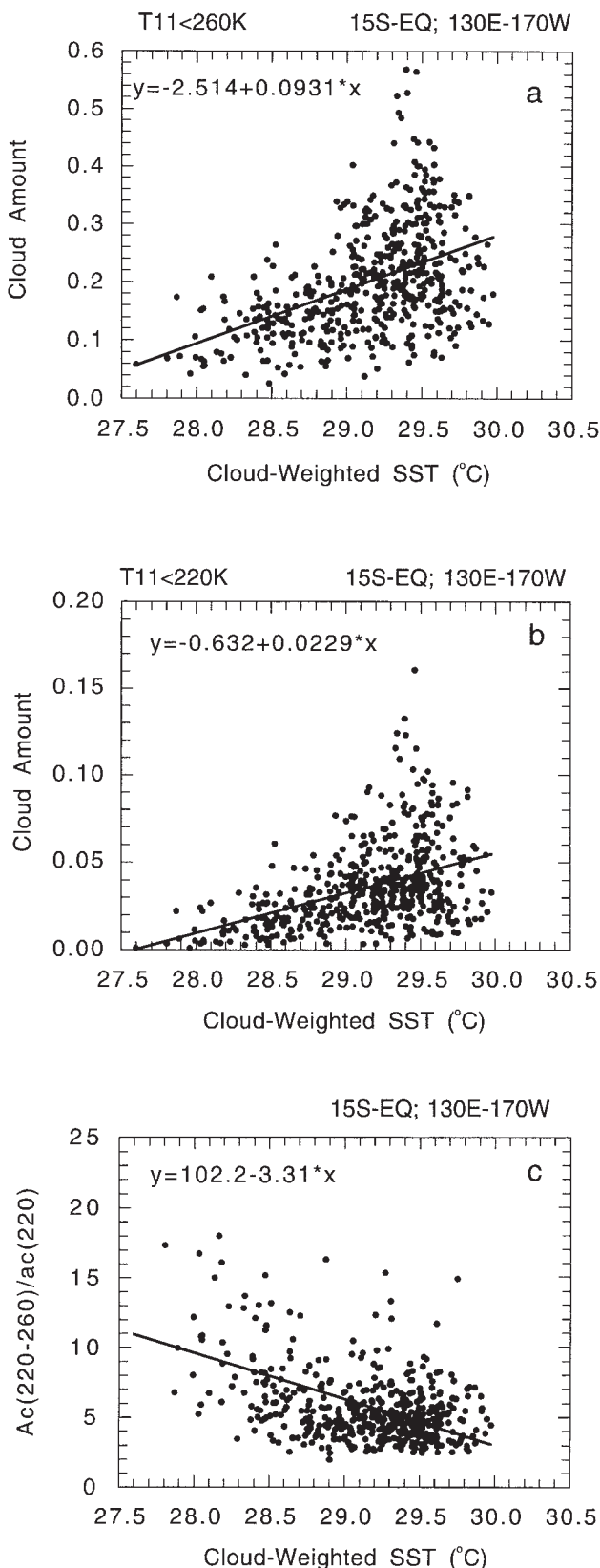


FIG. 6. (a), (b) Scatterplots showing how cirrus and cumulus coverage varies with cloud-weighted SST for a subregion of Fig. 4 (15°S–equator, 130°E–170°W); (c) also the variation of cirrus coverage normalized by cumulus coverage with cloud-weighted SST. (See text for details.)

suggest a somewhat greater effect than was directly inferred from Fig. 5d. However, for subsequent calculations, we will stick with the smaller estimate.

A final alternative to be considered is that the observed high stratiform cloud cover is largely unconnected to convection, as might occur if there were incursions of stratiform systems from the extratropics. In such a case, the conceptual picture illustrated in Fig. 2 would be inappropriate. Apart from the fact that this is largely inconsistent with the full results we have presented, it would also lead to dependence on cloud-weighted SST being different depending on whether the weighting was based on high stratiform clouds or on cumulus. While the behavior is close, we are examining this matter in greater detail.

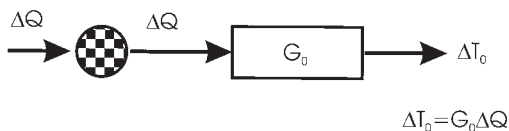
Finally, we should also note that cloud-weighted SST varies much more with time than either SST or mean SST. The fact that cloud microphysics depends on cloud-weighted SST gives us a much larger dynamic range to examine, which, in turn, is important for reliable determination of the effect of cloud-weighted SST. That said, it bears repeating that cirrus detrainment cannot depend on surface temperature alone. What we have attempted to do is to isolate that part of the dependence which is on SST.

In view of the above discussion, we feel that it is a plausible possibility that we are looking at a temperature dependence of detrainment, and we turn next to examining the potential radiative implications of such pronounced changes in the area of the moist regions. This is as much an exercise to determine whether the iris mechanism is capable, even in principle, of being significant, as an attempt to determine climate sensitivity.

4. Simple radiative-convective assessment of feedback

Before calculating the implications of the above for feedbacks, it is important to understand feedbacks more generally. Figure 7a shows a schematic for the behavior of the climate system in the absence of feedbacks. The circle simply represents a node, while the box represents the climate system that is characterized by a no-feedback gain, G_0 . The climate system acts on a radiative forcing, ΔQ , to produce a no-feedback response, $\Delta T_0 = G_0 \Delta Q$. Figure 7b shows the situation when a feedback process is present. Here, an additional forcing flux is produced that is proportional to the response, ΔT . This flux is written $F\Delta T$ and is added to

a. No Feedback Case



b. Feedback Case

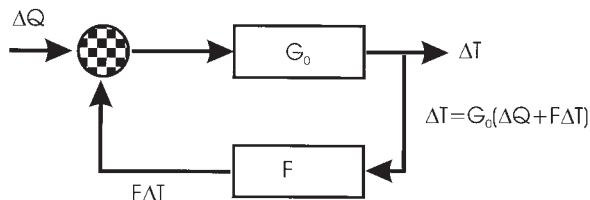
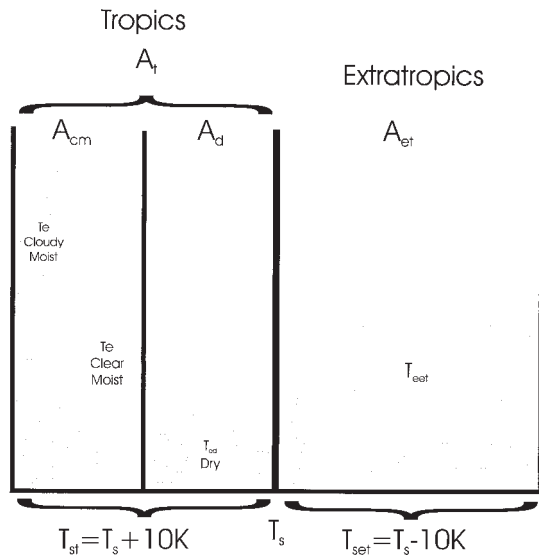


FIG. 7. Schematic illustrating operation of feedbacks.

the external forcing, ΔQ . The response is now, $\Delta T = G_0(\Delta Q + F\Delta T)$. The quantity $G_0 F \Delta T$ is the (no feedback) system response to the feedback flux, $F\Delta T$. Solving for ΔT , one gets $\Delta T = G_0 \Delta Q / (1 - G_0 F) = \Delta T_0 / (1 - G_0 F)$. The quantity $G_0 F$ is sometimes referred to as the feedback factor, f ; it is simply the response of the climate system to the feedback flux (nondimensionalized by 1°C) resulting from $\Delta T = 1\text{C}$. In the present case, this is associated with 22% reduction in the area of tropical upper-level cirrus. Note, that the *net* response, ΔT , is not the same as the response to the feedback flux alone. Note as well, that if there are several independent feedbacks, each will contribute its flux additively to the node, and f is replaced by $\sum f_i$.

Thus, to evaluate the feedback factor due to changing the relative area of the moist region, we must calculate the response of the climate system to such changes. This is readily dealt with using a very simple model. We divide the world into three regions: the moist Tropics, the dry Tropics, and the extratropics. For purposes of evaluating outgoing longwave radiation (OLR), we further divide the moist region of the Tropics into a cloudy–moist region covered by upper-level cirrus, and a clear–moist region clear of such cirrus. For this reason, we refer to the model as a 3.5-box model. This approach to the Tropics is supported by the sharp transitions illustrated in Fig. 1. The model is illustrated in Fig. 8. We take each region to have a lapse rate of 6.5 K km^{-1} . The use of a moist adiabat would certainly be more accurate, but would make little difference for the present calculations. Both tropical regions are taken to have cloud-capped trade cumulus boundary layers. Also, the tropical regions are both taken to have characteristic surface temperatures



Simple 3.5-box model for the Greenhouse Effect due to clouds and water vapor

FIG. 8. The 3.5-region model for two-dimensional calculation of radiative-convective equilibrium. Symbols are defined in Table 1.

that are 10 K warmer than the mean surface temperature, while the extratropical region is taken to have a characteristic surface temperature 10 K colder than the mean surface temperature. (In models, at least, there are amplified high-latitude responses, but these are restricted to small areas, and make little difference to extratropical means.) We assume the current value of moist fractional area to be 0.25, and choose the remaining parameters so as to be consistent with the global mean temperature, T_s , being 288 K, and match Earth Radiation Budget Experiment (ERB) observations (Barkstrom 1984), which show a planetary reflectivity of 0.308, a tropical clear sky reflectivity of 0.13, a tropical reflectivity of 0.241, an extratropical reflectivity of 0.403, a planetary emission temperature of 254 K, a tropical emission temperature of 259.1 K, and an extratropical emission temperature of 249 K. The moist region is taken to have high relative humidity and high-altitude cirrus, both of which lead to elevated characteristic emission levels. Consistent with ERBE, the OLR from tropical dry regions is about 303 W m^{-2} corresponding to an emission temperature of about 270 K (and a characteristic emission level of a little over 4 km). From both ERBE and radiative calculations, the OLR from clear-moist regions is about 263 W m^{-2} , corresponding to an emission temperature

of about 261 K (and a characteristic emission level of about 5.7 km). Consistency with ERBE full sky OLR for the Tropics then requires that OLR from the cloudy moist area of the Tropics be about 138 W m^{-2} , corresponding to an emission temperature of about 222 K (and a characteristic emission level of about 11.7 km). The characteristic emission level of the extratropics is taken to be at 4.5 km. The complete choice of parameters is given in Table 1. Although ERBE values do not completely constrain these choices, the precise choice of most individual parameters did not matter much to our final results as long as ERBE values were approximately matched. This is particularly true for the choice of the current value of the moist fractional area as well as the fractional portion of this area covered by upper-level cirrus. Whatever values we chose for these, once tuned to match ERBE (full sky) results, led to similar results when perturbed. Finally, we should note that for purposes of calculating reflectivity in the Tropics, we allow for random overlap of upper- and lower-level clouds. Therefore, we must distinguish (A) regions with only upper-level clouds, (B) regions with both upper and lower-level clouds, (C) regions with only lower-level clouds, and (D) cloud-free regions. This is illustrated in Fig. 9.

The information in Table 1 permits us to calculate total reflectivity in each of the regions, from which we can then calculate the net incoming solar radiation: net incoming solar radiation = $Q = Q_0(Q_t(A_{cm}(1 - \text{tr}_{cm}) + A_d(1 - \text{tr}_d)) + A_{et}Q_{et}(1 - \text{tr}_{et}))$, and net reflectivity will simply be $(1 - Q/Q_0)$.

The net OLR consists simply in Planck blackbody emission from the characteristic emission levels in the four regions:

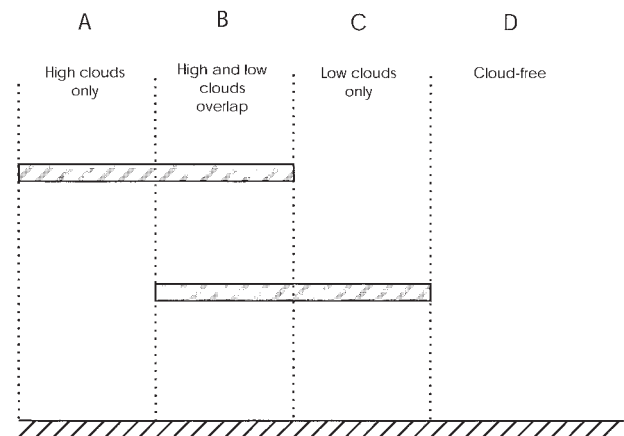


FIG. 9. Different arrangements of stratiform clouds considered. (See text for details.)

TABLE 1. Parameter selection in 3.5-box greenhouse model.

Parameter	Description	Value
A_{cm}	Relative area of tropical moist region	0.25
A_t	Relative area of the Tropics	0.5
$A_d = A_t - A_{cm}$	Relative area of tropical dry region	0.25
$A_{et} = 1 - A_t$	Relative area of extratropics	0.5
f_h	Fractional coverage of high tropical clouds (within moist region)	0.44
$A_{cloudymoist} = f_h A_{cm}$	Relative area of cloudy tropical moist region	0.11
$A_{clearmoist} = (1 - f_h) A_{cm}$	Relative area of clear tropical moist region	0.14
$f_{tropicalcloud} = f_h A_{cm} / A_t$	Tropical cloud fraction	0.22
r_h	Reflectivity of high tropical clouds	0.24
f_l	Fractional coverage of tropical low cloud (trade cumuli, etc.)	0.25
r_l	Reflectivity of tropical low clouds	0.42
r_{bt}	Clear sky reflectivity in the Tropics	0.13
$t_h = 1 - (r_h + 0.07)$	Transmissivity of high clouds (allowing for absorption)	
$t_l = 1 - (r_l + 0.07)$	Transmissivity of low clouds (allowing for absorption)	
$r_{hl} = r_h + \left[t_h^2 \frac{r_l}{1 - r_h r_l} \right]$	Reflectivity due to overlapping high and low clouds	
$t_{hl} = \frac{t_h t_l}{1 - r_h r_l}$	Transmissivity due to overlapping high and low clouds	
$r_A = r_h + \frac{t_h^2 r_{bt}}{1 - r_h r_{bt}}$	Total reflectivity for region A in Fig. 9	
$r_B = r_{hl} + \frac{t_{hl}^2 r_{bt}}{1 - r_{hl} r_{bt}}$	Total reflectivity for region B in Fig. 9	
$r_C = r_l + \frac{t_l^2 r_{bt}}{1 - r_l r_{bt}}$	Total reflectivity for region C in Fig. 9	
$r_D = r_{bt}$	Total reflectivity for region D in Fig. 9	

TABLE 1. *Continued.*

Parameter	Description	Value
$f_{\text{icm}} = f_h + (1 - f_h)f_l$	Fractional cloud coverage for tropical moist area	
$tr_{\text{cm}} = f_h(1 - f_l)r_A + f_h f_l r_B + (1 - f_h)f_l r_c + (1 - f_{\text{icm}})r_D$	Total reflectivity for tropical moist area	
$tr_d = f_l r_c + (1 - f_l)r_D$	Total reflectivity for tropical dry area	
$tr_{\text{tropics}} = \frac{A_{\text{cm}} tr_{\text{cm}} + A_d tr_d}{A_{\text{cm}} + A_d}$	Total reflectivity for the Tropics	0.242
tr_{et}	Total reflectivity for the extratropics	0.403
T_s	Mean surface temperature	
$T_{\text{st}} = T_s + 10\text{K}$	Tropical surface temperature	
$T_{\text{set}} = T_s - 10\text{K}$	Extratropical surface temperature	
$T_{\text{ecloudy moist}} = T_{\text{st}} - 76\text{K}$	Emission temperature from tropical cloudy–moist region	
$T_{\text{eclear moist}} = T_{\text{st}} - 37\text{K}$	Emission temperature from tropical clear–moist region	
$T_{\text{ed}} = T_{\text{st}} - 27.6\text{K}$	Emission temperature from tropical dry region	
$T_{\text{eet}} = T_{\text{set}} - 29.3\text{K}$	Emission temperature from extratropics	
Q_0	Mean solar irradiation	$\sigma(254\text{K})^4/(1 - 0.308)$
Q_t	Relative solar irradiation in Tropics	1.174
Q_{et}	Relative solar irradiation in extratropics	0.826

net OLR =

$$C(T_s) = \sigma(A_{\text{cloudy moist}} T_{\text{ecloudy moist}}^4 + A_{\text{clear moist}} T_{\text{eclear moist}}^4 + A_d T_d^4 + A_{\text{et}} T_{\text{eet}}^4).$$

Note that convective adjustment, here, consists of fixing the relation between surface temperature and the temperature at the characteristic emission levels.

Finally, we obtain the mean surface temperature by equating net incoming solar radiation to net OLR:

$$C(T_s) = Q \Rightarrow T_s.$$

Having tuned our simple model to replicate ERBE measurements, we proceed to vary $f_{\text{tropical cloud}}$. Although we have argued that the area of moist air, A_{cm} , should follow $f_{\text{tropical cloud}}$, it is only the latter that has been observed. Thus, we take $F_{\text{tropical cloud}} = 0.22(1 + \mu)$, letting μ range from -0.3 to $+0.3$. We also take $A_{\text{cm}} = 0.25(1 + \gamma\mu)$. If A_{cm} follows the area of cloudy moist air, then $\gamma = 1$. However, we also examine results for $\gamma = 0.5$ and 0 . (This issue is being separately examined using CERES data from TRMM; preliminary results suggest $\gamma \approx 0.75$). Everything else is held constant. In particular, the amount of cumulus convection is assumed to be constant so that the relation between $f_{\text{tropical cloud}}$ and

cloud-weighted SST should be proportional to the dependence shown in Fig. 5d.

Figure 10 shows how global mean temperature varies with the area of tropical upper-level cloud. Also shown in Fig. 10 is the variation of global reflectivity. The latter varies fairly little since substantial reflectivity is due to the clouds capping the boundary layer and to the surface reflectivity. However, the global mean radiative–convective surface temperature varies substantially indicating the dominance of the infrared effect of the moist region. Under the interpretation of the observations in section 3, that the changing upper-level cloud area is due to the changing cloud-weighted temperature per se, then the cloud area changes 22% for a 1°C change in cloud-weighted SST (Fig. 5d). Under conditions of global warming, we assume that both global mean temperature and cloud-weighted surface temperature increase together. As already explained, the response of T_s to this change in cloud area will constitute the feedback factor (G_0F or f). Roughly speaking, a 22% reduction in this area (from a base of about 0.22) leads to about a 1.1°C reduction in global mean temperature for $\gamma = 1$, 0.7°C for $\gamma = 0.5$, and 0.45°C for $\gamma = 0$, implying feedback factors of -1.1 , -0.7 , and -0.45 . *Essentially, the cloudy–moist region appears to act as an infrared adaptive iris that opens up and closes down the regions free of upper-level clouds, which more effectively permit infrared cooling, in such a manner as to resist changes in tropical surface temperature. Moreover, on physical and observational grounds, it appears that the same applies to moist and dry regions.* Our model includes the fact that dynamics ties temperatures everywhere together and determines the mean meridional gradient. The feedback factor is for the effect of the Tropics on the global mean. Thus, the

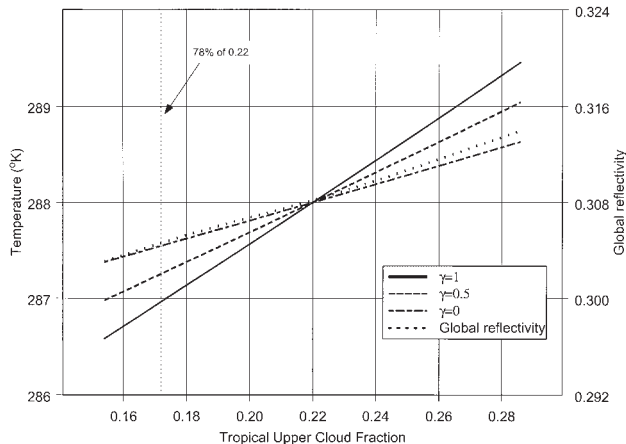


FIG. 10. Calculated variation of global mean temperature, T_s vs area (relative to the Tropics) of the tropical cloudy region. The curves for different γ 's correspond to the different degrees to which the area of moist air, A_{cm} , might follow the area of cloudy air. Here, $\gamma = 1$ corresponds to both changing together, while $\gamma = 0$ corresponds to the area of moist air remaining unchanged. (See text for details.)

response to a doubling of CO_2 , which in the absence of feedbacks is expected to be about 1.2°C, would be reduced to between 0.57° and 0.83°C (depending on γ) due to the iris effect.

In some respects, the iris effect can be considered to be independent of the positive feedbacks found in current models. The response of current climate GCMs to a doubling of CO_2 ranges from 1.5° to 4°C. This corresponds to positive feedback factors ranging from 0.2 to 0.7 [with the model water vapor feedback factor typically contributing 0.4; Lindzen (1993); Schneider et al. (1999)]. The inclusion of the iris feedback more than cancels the model positive feedbacks in most cases. This is illustrated in Table 2. (Note that although we retain three significant figures for conve-

TABLE 2. Modification of climate sensitivity in presence of both model feedbacks and various modifications of the iris feedback.

Iris feedback factor (f)	GCM feedback factor (f) (high)	GCM feedback factor (f) (low)	Total feedback factor (f) (high)	Total feedback factor (f) (low)	Net gain $1/(1-f)$ (high)	Net gain $1/(1-f)$ (low)	Response to $2 \times \text{CO}_2$ (°C) (high)	Response to $2 \times \text{CO}_2$ (°C) (low)
-1.1	0.7	0.2	-0.4	-0.9	0.71	0.53	0.852	0.636
-0.7	0.7	0.2	-0.0	-0.5	1.0	0.67	1.2	0.804
-0.45	0.7	0.2	0.25	-0.25	1.33	0.8	1.596	0.96

nience in computation, nothing in the data suggests this level of accuracy.)

The iris effect acts to reduce the sensitivities from the range, 1.5° – 4°C , to the range 0.64° – 1.6°C . The reduced sensitivity is within the range of many sensitivity estimates including the relatively low estimates obtained from the observed response to a sequence of volcanoes by Lindzen and Giannitsis (1998) and the more conventional estimate of North and Wu (2001). This, however, is not meant to suggest that the range of feedbacks found in present models is necessarily correct. Rather it is meant to show the impact that the iris effect would have on these model results.

5. GCM assessment

The present results suggest a useful set of diagnostics to be applied to GCMs. A preliminary attempt to replicate the presence of the feedback using a GCM consisting in the National Center for Atmospheric Research (NCAR) Community Climate Model, version 3.3.6 (CCM3), physics and a dynamic core developed by S. J. Lin at the National Aeronautics and Space Administration (NASA) Goddard Space Flight Center, forced by the same SST data used for the observational analysis, fails to indicate its presence. The GCM study is based on comparison of the high cloud fraction generated by the CCM3 physics, which consist of random-overlapping convective clouds and humidity-dependent layered clouds between 50 and 400 hPa (see NCAR 2000). A comparison of observational and model results for the period May–June 1998 is given in Fig. 11. The GCM scatter suggests no systematic response of cloud area to cloud-weighted SST although the formal regression actually suggests a positive rather than a negative dependence. Comparisons with other models [the Center for Ocean–Land–Atmosphere Studies (COLA) and several versions of NCAR’s CCM3 models have been examined so far] also show profound differences from observations regardless of whether diagnostic or prognostic cloud formulations were used. However, the modes of failure differ somewhat from model to model. Detailed comparisons will be made in a separate paper in which we hope to have additional model comparisons.

The failure of models to replicate observed relations between upper-level cloud coverage and cloud-weighted SST is important for such matters as coupling between the atmosphere and the surface quite

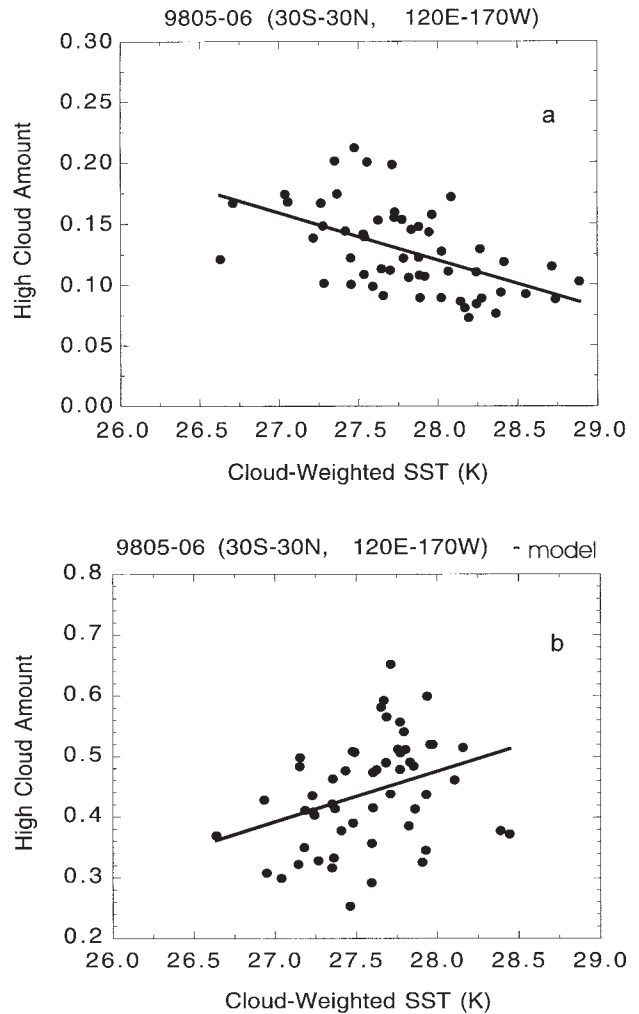


FIG. 11. Scatterplots showing how cirrus coverage varies with cloud-weighted SST for both observations and the Data Assimilation Office climate GCM forced by the SST. (See text for details.)

apart from implications for climate sensitivity. From the existing literature, moreover, we know that at least some models fail to show the sharp delineation between moist and dry regions, and underestimate the differences between dry and moist regions (Roca et al. 1997).

6. Discussion

Given the limited period and region considered as well as the incompleteness of spectral data at suitable spectral, temporal, and spatial resolution, and the limitations of the SST data, in addition to the possibility of alternative explanations of the data, the present results must still be regarded as tentative at best. There remain, as well, the possibilities that under conditions

of global warming due to increasing CO₂, CAPE might change as might the amount of convection (although the present results suggest that the second possibility is small unless accompanied by changes in the pattern of SST). If CAPE increases, the time available for rain formation would decrease, and this might diminish the present feedback. There are indeed arguments and observations that suggest modest increases for warmer climates (Emanuel and Bister 1996; Rennó 1997). Nonetheless, given the low climate sensitivity implied by the iris effect, and the plausible expectation that differences in CAPE comparable to what might be expected from future climate change are to be found within the region shown in Fig. 4, we would not expect the iris effect to be significantly reduced under conditions of doubled CO₂.¹

We are thus left with evidence for a potentially effective negative feedback in the Tropics. In the absence of changes in those processes that have a major effect on the equator-to-pole heat flux, this also inhibits global change. This was the situation assumed in section 4. The existence of global change, whose existence is amply recorded in the paleoclimatic record, would, if the feedback described in this paper proves correct, demand changes in those factors that determine the equator-to-pole temperature difference as noted in Lindzen (1993). Examples are changes in the intensity of the Hadley supply of momentum to the subtropical jet (Lindzen and Pan 1994; Hou 1998) and changes in the differential heating as might be produced by large-scale high-latitude snow cover or changes in the ocean heat transport. In the presence of a strong negative feedback in the Tropics, such changes would also be accompanied by changes in global mean temperature, but the primary characteristic of such climate change would be the change in equator-to-pole temperature difference.

On shorter timescales, there are changes in SST pattern such as ENSO that appear to alter the equator-to-pole heat flux. The existence of a strong negative feedback in the Tropics will again act in such a man-

ner as to translate changes in the dynamic heat flux between the Tropics and the extratropics into changes in the global mean temperature rather than simple self-canceling changes in the Tropics and extratropics. Thus, it is by no means clear that the thermostatic process described in this paper would not increase natural variability in global mean temperature—in contrast to the findings of Hall and Manabe (1999).

Whether the iris feedback ultimately proves as effective as our results suggest, the inability of existing models to replicate the relevant observations suggests the need for model improvement in an area potentially crucial to the determination of climate sensitivity. It also suggests that the range of climate sensitivity found in current models need not constrain the real range—especially at the low end. The present results suggest the importance of improved data (including, e.g., 183-GHz sounders on geostationary satellites so as to obtain observations of water vapor at the same time and space resolution as the cloud data) in order to more firmly identify the nature and magnitude of the feedback described in the present paper. Finally, it would be interesting to develop a parameterization of the process discussed in this paper for implementation in a GCM so as to see how the climate behavior of the model would be altered. This would address the challenge put forth in Held and Soden (2000); namely that explicit processes be suggested that might reduce the water vapor feedback so that these processes could be checked in GCMs. It would, of course, be of interest to see how model climate sensitivity is affected. However, as noted earlier, it is likely to be of comparable interest to see how the parameterization affects such matters as air–sea coupling and climate drift.

Acknowledgments. The efforts of R. S. Lindzen were supported by Grants ATM9813795 from the National Science Foundation, DEFG02-93ER61673 from the Department of Energy, and NAG5-5147 from the National Aeronautics and Space Administration. The work of M.-D. Chou was supported by the Radiation Research Program, NASA/Office of Earth Science. We would like to thank Dr. S. J. Lin and Ms. Sharon Nebuda for providing the NASA–NCAR results used in Fig. 11; Drs. E. Schneider and B. Boville for assessment of the COLA and NCAR models, respectively, for our mechanism; and D. Kirk-Davidoff, K. Emanuel, I. M. Held, R. Pierrehumbert, and an anonymous reviewer for helpful comments.

References

- Barkstrom, B. R., 1984: The Earth Radiation Budget Experiment (ERBE). *Bull. Amer. Meteor. Soc.*, **65**, 1170–1185.

¹It has been suggested by I. M. Held (2000, personal communication) that cloud-weighted SST in the present study might simply be indicating changes in CAPE, and that the area effect we are observing is due to CAPE rather than temperature per se. As already noted measurement of CAPE is by no means trivial. Thus, this possibility cannot be ruled out. Nonetheless, it would require that CAPE decrease with increasing cloud-weighted SST so as to allow greater precipitation efficiency within cumuli. This seems to be counter to most current expectations.

- Betts, A. K., 1990: Greenhouse warming and the tropical water budget. *Bull. Amer. Meteor. Soc.*, **71**, 1464–1465.
- Emanuel, K. A., and M. Bister, 1996: Moist convective velocity and buoyancy scales. *J. Atmos. Sci.*, **53**, 3276–3285.
- , and R. T. Pierrehumbert, 1996: Microphysical and dynamical control of tropospheric water vapor. *Clouds, Chemistry and Climate*, P. J. Crutzen and V. Ramanathan, Eds., NATO ASI Series, No. 135, Springer-Verlag, 17–28.
- Fairall, C. W., E. F. Bradley, D. P. Rogers, J. B. Edson, and G. S. Young, 1996: Bulk parameterization of air–sea fluxes for TOGA COARE. *J. Geophys. Res.*, **101**, 3747–3764.
- Gamache, J. F., and R. A. Houze, 1983: Water budget of a meso-scale convective system in the tropics. *J. Atmos. Sci.*, **40**, 1835–1850.
- Hall, A., and S. Manabe, 1999: The role of water vapor feedback in unperturbed climate variability and global warming. *J. Climate*, **12**, 2327–2346.
- Held, I. M., and B. Soden, 2000: Water vapor feedback and global warming. *Annu. Rev. Energy Environ.*, **25**, 441–475.
- Hou, A. Y., 1998: Hadley circulation as a modulator of the extra-tropical climate. *J. Atmos. Sci.*, **55**, 2437–2457.
- Lindzen, R. S., 1990: Response. *Bull. Amer. Meteor. Soc.*, **71**, 1465–1467.
- , 1993: Climate dynamics and global change. *Annu. Rev. Fluid Mech.*, **26**, 353–378.
- , and S. Nigam, 1987: On the role of sea surface temperature gradients in forcing low level winds and convergence in the tropics. *J. Atmos. Sci.*, **44**, 2418–2436.
- , and W. Pan, 1994: A note on orbital control of equator–pole heat fluxes. *Climate Dyn.*, **10**, 49–57.
- , and C. Giannitsis, 1998: On the climatic implications of volcanic cooling. *J. Geophys. Res.*, **103**, 5929–5941.
- Manabe, S., and R. T. Wetherald, 1967: Thermal equilibrium of the atmosphere with a given distribution of relative humidity. *J. Atmos. Sci.*, **24**, 241–259.
- Miller, R., and R. S. Lindzen, 1992: Organization of rainfall by an unstable jet with application to African waves. *J. Atmos. Sci.*, **49**, 1523–1540.
- NCAR, cited 2000: The NCAR Community Climate Model (CCMS) users’ guide. [Available online at <http://www.cgd.ucar.edu/cms/ccm3/>]
- North, G. R., and Q. Wu, 2001: Detecting climate signals using space–time EOFs. *J. Climate*, in press.
- Pierrehumbert, R. T., 1995: Thermostats, radiator fins, and the local runaway greenhouse. *J. Atmos. Sci.*, **52**, 1784–1806.
- , and R. Roca, 1998: Evidence for control of Atlantic subtropical humidity by large scale advection. *Geophys. Res. Lett.*, **25**, 4537–4540.
- Prabhakara, C., D. P. Kratz, J.-M. Yoo, G. Dalu, and A. Vernekar, 1993: Optically thin cirrus clouds: Radiative impact on the warm pool. *J. Quant. Spectrosc. Radiat. Transfer*, **49**, 467–483.
- Rennó, N. O., 1997: Multiple equilibria in radiative-convective atmospheres. *Tellus*, **49A**, 423–438.
- Reynolds, R. W., and T. M. Smith, 1994: Improved global sea surface temperature analyses. *J. Climate*, **7**, 929–948.
- Riehl, H., and J. S. Malkus, 1958: On the heat balance in the equatorial trough zone. *Geophysica* (Helsinki), **6**, 503–538.
- Roca, R., L. Picon, M. Desbois, and H. Le Treut, 1997: Direct comparison of Meteosat water vapor channel data and general circulation model results. *Geophys. Res. Lett.*, **24**, 147–150.
- Rogers, R. R., and M. K. Yau, 1989: *A Short Course in Cloud Physics*. Pergamon Press, 293 pp.
- Salathé, E. P., and D. L. Hartmann, 1997: A trajectory analysis of tropical upper-tropospheric moisture and convection. *J. Climate*, **10**, 2533–2547.
- Schneider, E. K., B. P. Kirtman, and R. S. Lindzen, 1999: Upper tropospheric water vapor and climate sensitivity. *J. Atmos. Sci.*, **56**, 1649–1658.
- Sherwood, S. C., 1996: Maintenance of free-tropospheric water vapor distribution. Part II: Simulation by large-scale advection. *J. Climate*, **9**, 2919–2934.
- Soden, B. J., 1998: Tracking upper tropospheric water vapor. *J. Geophys. Res.*, **103**, 17 069–17 081.
- Spencer, R. W., and W. D. Braswell, 1997: How dry is the tropical free troposphere? Implications for global warming theory. *Bull. Amer. Meteor. Soc.*, **78**, 1097–1106.
- Stephens, G. L., D. L. Jackson, and I. Wittmeyer, 1996: Global observations of upper tropospheric water vapor derived from TOVS radiance data. *J. Climate*, **9**, 305–326.
- Straus, D., and R. S. Lindzen, 2000: Planetary-scale baroclinic instability and the MJO. *J. Atmos. Sci.*, **57**, 3609–3626.
- Sun, D.-Z., and R. S. Lindzen, 1993: Distribution of tropical tropospheric water vapor. *J. Atmos. Sci.*, **50**, 1643–1660.
- Udelhofen, P. M., and D. L. Hartmann, 1995: Influence of tropical cloud systems on the relative humidity in the upper troposphere. *J. Geophys. Res.*, **100**, 7423–7440.

